PAPER

Trimodal hierarchical carbide-derived carbon monoliths from steam- and CO_2-activated wood templates for high rate lithium sulfur batteries†

Marion Adam,[a] Patrick Strubel,[b] Lars Borchardt,[a] Holger Althues,[b] Susanne Dörfler[b] and Stefan Kaskel*[ab]

Hierarchically structured biomorphic carbide-derived carbon (CDC) materials are obtained by applying a combined activation- and CDC approach on abundantly available, renewable and cheap raw materials. For the synthesis of these materials we mimic nature by using wood structures as templates which are already optimized for mass transport during their long-term evolutional process. The impregnation of steam- or carbon dioxide-pre-activated wood templates with a polycarbosilane precursor and the subsequent halogen treatment yields a hierarchical material that exhibits longitudinally orientated macropores from the wood structure as well as well-defined and narrowly distributed micro- and meso-pores derived from the activation and CDC approach. These materials offer specific surface areas up to 1750 $m^2 g^{-1}$, micro-/meso-pore volumes up to 1.0 $cm^3 g^{-1}$ and macropore volumes of 1.2 $cm^3 g^{-1}$. This sophisticated hierarchical pore system ensures both efficient mass transfer and high specific surface area, ideal for mass transport limited applications, such as the lithium sulfur battery. Testing steam activated wood-CDCs as cathode materials for Li−S batteries reveals excellent performance, especially a highly stable discharge capacity and sulfur utilization. Stable capacities of over 580 mA h g_{sulfur}^{-1} at current densities exceeding 20 mA cm^{-2} (2C) are possible using only very low amounts of electrolyte of 6.8 µL mg_{sulfur}^{-1}.

Introduction

Porous carbon materials have gained considerable attention in the last few years due to their high chemical and thermal stability, tunable pore size distribution, and high specific surface areas (SSAs), which lead to a wide range of potential applications, such as catalysis,[1,2] gas separation/adsorption,[3,4] and electrochemical energy storage.[5,6]

However, in many applications a high specific surface area combined with advanced mass transport kinetics is of great interest. Therefore, the focus in the last few years is on the synthesis of hierarchically structured carbons, where meso- or macro-pores can be achieved *via* various template concepts.[1,7–9] These approaches tend to be complex, laborious, time-consuming and the template itself often has to be expensively synthesized. Under these considerations, natural templates[10–16] offer several advantages, such as abundant availability,

renewability and considerably low price. Moreover, bio-templates like wood already possess a hierarchical cell anatomy that is optimized for mass transport during a long-term evolutional process. This makes these materials particularly interesting for applications where enhanced mass transport kinetics are indispensable. However, besides a good transport pore system, high specific surface areas, usually provided by micro-pores, are highly desired for various applications. Much research has been carried out on chemical and physical activation of wood or wood-derived materials resulting in a variety of porous activated wood materials with high porosity.[17–21] Nevertheless, a high specific surface area can only be achieved at high activation levels, which involves a large destruction of the cell walls and a broad pore size distribution.[19,20]

The carbide-derived carbon (CDC) approach is a well-known possibility to obtain carbon materials with high SSA and a very narrow pore size distribution.[6,8,22] They are synthesized due to the selective removal of metal or semi-metal atoms from carbide precursors by hot halogen treatment. The porosity of CDCs can be controlled by the choice of the carbide precursor and the halogen treatment conditions.[23] Recently, we have shown that the combination of synthetic templates and the CDC approach allows access to hierarchical carbon materials with high SSAs (up to 3000 $m^2 g^{-1}$) and well-defined transport pore systems.[1,7,24] Hence, the use of biotemplates is the next step for synthesis of

[a]Department of Inorganic Chemistry, Dresden University of Technology, Bergstraße 66, 01062 Dresden, Germany. E-mail: stefan.kaskel@chemie.tu-Dresden.de; Tel: +49-35146333632

[b]Fraunhofer Institute of Material and Beam Technology, Winterbergstraße 28, 01277 Dresden, Germany

† Electronic supplementary information (ESI) available. See DOI: 10.1039/c5ta06782k

This journal is © The Royal Society of Chemistry 2015

J. Mater. Chem. A, 2015, **3**, 24103–24111 | **24103**

innovative materials. Combining the CDC approach and wood as a template is of considerable interest because the longitudinally orientated macropore system promotes high availability.

In a first proof-of-principle[25] we have recently shown that hierarchical wood-derived CDC materials can be synthesized. However, only moderate surface areas have been obtained and several infiltration steps or long infiltration times of the carbide precursor were necessary. Here we show how a pre-activation step with carbon dioxide or steam allows for both: higher surface areas and only a single impregnation step. We like to show that this preparation concept enables the combination of the benefits of the individual techniques with the wood template to produce carbon materials with high specific surface areas up to 1750 m^2 g^{-1} but also narrow nanopore size distribution. Hierarchical CDC materials with large transport pores can be synthesized, interesting as electrode materials for Li–S batteries, due to maintaining the unique wood microstructure with longitudinally orientated wood cells/macropores during the whole preparation process.

Sulfur is a cheap and non-toxic element with a high theoretical capacity of 1672 mA h g^{-1}.[26,27] However, despite intensive research focus in the last 10 years still challenges need to be addressed such as low sulfur utilization, cycle stability, coulombic efficiency as well as rate performance.[28] Introduced by Nazar's group in 2009, a large number of novel approaches have been explored to address the main disadvantages of Li–S batteries.[29–32] However, studies under practically relevant conditions, that are high sulfur loading, high electrode density, and low excess of electrolyte are rather scarce. This may play an important role at high C-rates due to the strong influence on the electrochemical kinetics. Hierarchical porous carbon materials having both *reaction*- and *transport*-pores may be advantageous because transport pores allow rapid ion transport (and thus faster charge–discharge rates), while micropores induce reduced polysulfide dissolution and provide high surface area for sufficient electrical contact between sulfur and carbon.[33,34] Hence, we will show that the activated wood-CDC material shows remarkable rate stability at high current densities exceeding 20 mA cm^{-2}, for application in lithium sulphur batteries.

Experimental

Materials synthesis

Preparation of biotemplate. Birch wood (*Betula verrucosa*) was used as a biotemplate for the synthesis of biomorphic CDC materials. The natural birch samples were cut into discs of approximately 1 g, 10 mm in diameter and 20 mm in height, cleaned from bark, and dried (80 °C, 24 h in air).

Steam activation. For steam activation, birch monoliths were placed in a horizontal quartz tube furnace and heated at a rate of 450 K h^{-1} from room temperature to 450 °C. At this temperature, the samples were treated with steam for 1.5 h. Steam was generated in the furnace by flushing with wet argon. Therefore, argon at a flowing rate of 80 mL min^{-1} was bubbled through deionized water in a heated flask. The water saturation of argon flow was adjusted with the water temperature of 25 °C,

50 °C, or 80 °C. After this treating step at 450 °C, the oven was heated to 900 °C in an argon atmosphere and kept at this point for 5 h with steam.

CO$_2$ activation. Prior to carbon dioxide activation, the birch monoliths were pyrolyzed in argon flow at 800 °C for 3 h. Afterwards, the activation experiments were carried out at 850 °C, 900 °C, and 950 °C for 2 h with carbon dioxide, heating with 100 K h^{-1} to desired temperature and cooling were performed under an argon atmosphere.

Synthesis of activated wood-CDCs. The activated wood monoliths were immersed with allylhydridopolycarbosilane (SMP-10, Starfire Systems) for 24 h at room temperature. The impregnated wood samples were dried overnight (80 °C in air) and then pyrolyzed (800 °C, 3 h under an argon flow, and 100 K h^{-1} heating rate) yielding bioC/SiC. Afterwards, a chlorine treatment was applied to remove silicon from SiC, yielding the activated wood-CDC. The samples were transferred in a horizontal quartz tube furnace and heated to 800 °C (450 K h^{-1} heating rate) with an argon flow of 150 mL min^{-1}. The gas flow was subsequently changed to a mixture of 80 mL min^{-1} chlorine and 70 mL min^{-1} argon while the temperature was maintained at the same level for 3 h. Finally, the chlorinated samples were treated with hydrogen for 1 h at 600 °C (80 mL min^{-1}) to remove residual chlorine species from the surface of the materials.

Nomenclature. The activated samples are specified with the activation method (CO$_2$ or H$_2$O) and the activation temperature in the case of carbon dioxide (850, 900 or 950) and the temperature of water in the case of steam activation (25, 50 or 80). The intermediate bioC/SiC is marked with –SiC and the resulting CDC materials with –CDC.

Material characterization

On an Autosorb 1C (Quantachrome Instruments) nitrogen physisorption measurements were performed at 77 K. SSAs were calculated using the Brunauer, Emmett and Teller (BET) equation in a relative pressure range of 0.05–0.20 p/p_0. Using the Quenched Solid Density Functional Theory (QSDFT) method for carbon (slit-cylindrical pores, adsorption branch kernel) the presented pore size distributions were calculated. Micropore volumes were calculated with QSDFT from the cumulative pore volumes at a pore diameter of 2 nm and total mesopore volumes at 30 nm pore diameter. Prior to nitrogen physisorption experiments, all samples were activated at 150 °C for 24 h under vacuum. Mercury intrusion porosity was calculated using a PASCAL440 (Thermo Fisher Scientific). Scanning electron microscopy (SEM) and energy dispersive X-ray analysis (EDX) were performed with a DSM-982 Gemini (Zeiss) at an acceleration voltage of 8 kV in the case of SEM and 20 kV in the case of EDX. Powder XRD was performed on an X'Pert diffractometer (PANalytical) in Bragg–Brentano geometry (Cu K$_{alpha}$ radiation, λ = 0.15405 nm). Thermal analyses were performed under ambient pressure in air or an inert atmosphere using a DTA-DSC Labsys TMA system (Setaram) with a heating rate of 5 K min^{-1}.

24104 | *J. Mater. Chem. A*, 2015, **3**, 24103–24111

This journal is © The Royal Society of Chemistry 2015

Electrochemical characterization

Composite preparation. The C/S composite was prepared by carefully mixing of the porous carbon material (reference material or H_2O50-CDC) and pristine sulfur (Sigma Aldrich, ≥99.5%) in a porcelain mortar. According to the different pore volumes, the weight ratio of carbon-to-sulfur was adjusted to 1 : 0.24 for reference and 1 : 0.34 for H_2O50-CDC. The sulfur was subsequently melt infiltrated at 155 °C for 12 h under air.

Electrode preparation. Cathodes were prepared from the C/S composites following a solvent-free roll-press procedure reported elsewhere.[35] The C/S composite was mixed with carbon nanotubes as a conductive additive and PTFE binder in a weight ratio of 85 : 12 : 3. The typical active material loading of the punched circular electrodes with a diameter of 12 mm is 2–3 mg_{sulfur} cm^{-2}.

Electrochemical characterization. Lithium–sulfur half cells were prepared in an argon filled glove box (MBraun, <0.1 ppm O_2 and <0.1 ppm H_2O) by stacking the C/S composite cathode (working electrode), a porous polypropylene separator (Celgard 2500) and elemental lithium (MTI Corp., counter and reference electrode) with 6.8 μL mg_{sulfur}^{-1} of electrolyte in CR2016 coin cells. The electrolyte consisted of 1 M LiTFSI and 0.25 M $LiNO_3$ in DME/DOL (dimethoxy ethane/1,3-dioxolane) (1 : 1 by volume). The rate capability tests at different discharge rates (discharge//charge rate of C/10//C/10; C/5//C/5; C/2//C/5; 1C//C/5; 2C//C/5; 5C//C/5; 1C = 1672 mA g_{sulfur}^{-1}) were characterized at room temperature with a BASYTEC CTS cell test system. For increased polarization, the typical voltage range of 1.8–2.6 V *vs.* Li/Li⁺ was readjusted to 1.6–2.6 V *vs.* Li/Li⁺ at a discharge rate of C/2 and to 1.4–2.6 V *vs.* Li/Li⁺ at high discharge rates of 1C and 2C as well as to 1.2–2.6 V *vs.* Li/Li⁺ at 5C.

Results and discussion

Structure and porosity of activated wood-CDC

Hierarchically structured, activated wood-carbide-derived carbons were synthesized *via* activation of the bio-template with steam or carbon dioxide and a subsequent CDC approach, as shown in Fig. 1. In contrast to already known synthetic templates used for the synthesis of hierarchical carbon structures such as DUT-86[36] or polyHIPE-CDC,[24] no time-consuming template synthesis and their removal is necessary. Furthermore, wood offers a macroporous structure, which enables the possibility to produce sustainable, hierarchical porous carbon materials with 300–30 000-fold lower costs.

Biotemplate activation

Activated carbon monoliths were produced by treating wood monoliths at 900 °C with varying concentrations of water steam or at different temperatures with carbon dioxide. Weight losses (burn off), specific surface areas, pore volumes, and pore sizes of resulting activated wood monoliths are shown in Table 1.

The higher the carbonization temperature/the steam concentration, the higher the gasification amount, caused by the Boudouard equation (CO_2 + C ↔ 2CO, $\Delta_R H$ = +172.5 kJ mol^{-1}) and/or the progressive partial oxidation of the carbon

structure in both activation processes. SEM images in Fig. 2 and 3 show that gasification of carbon partially damaged the cell walls, inducing many micro- and meso-pores while preserving the unique cell structure of wood with longitudinally directed macropores and the monolithic structure. Pore size distributions (Fig. 4 and 5) calculated with the QSDFT method from low pressure nitrogen physisorption isotherms show the presence of a hierarchical micro-/meso-type pore system. In combination with the SEM images showing the preservation of macropores of about 4 μm (Fig. 2 and 3), we could demonstrate the synthesis of a carbon material with a trimodal pore system. Due to the pore formation by the activation process, bioC monoliths with SSAs up to 815 m^2 g^{-1} in the case of steam activation and 1080 m^2 g^{-1} in the case of carbon dioxide activation can be obtained. The SSAs of synthesized steam activated monoliths are in the same range as those of the activated wood powders discussed in the literature.[20,21] Hence, we could demonstrate that the utilization of monoliths in activation processes is also possible. As described before, steam activation under various conditions is performed in the literature. Wu *et al.*[20] synthesized activated fir wood carbon under same conditions with a slightly higher SSA but significant lower micropore amounts of only 51% of the total micro-/meso-pore volume in contrast to 61–78% for the steam activated wood samples presented here. Due to a reduced diffusion of the activating gas within the monoliths in comparison to powders, the activation process is less progressed explaining that the amount of micropores stays fairly above the values in the cited literature.

The specific surface area of the resulting steam activated carbon materials increases when the water temperature is increased up to 50 °C. A further increase in the steam concentration leads to higher burn off, which results in progressive destruction of the wood walls and widening of the formed pores, resulting in a smaller SSA and higher mesopore volume. The determined nitrogen physisorption isotherms of type IV according to the IUPAC classification (Fig. 4) show broadening hysteresis loops with higher water concentrations, which imply the increasing presence of mesopores in the activated bioC structures. Regarding the pores size distributions, a significant increase of the small mesopores of 2 to 10 nm with increasing water content is observed, which explains the decreasing micropore amounts from 78 to 61% ($V_{micro}/V_{micro+meso}$).

In this respect, the key challenge of this method is the optimization of the SSA, finding the right steam concentration/water temperature, where the gasification rate is high enough to introduce a huge number of micropores but not too high, preventing a pronounced destruction of the bioC. According to our results, 50 °C seems to be an appropriate temperature to meet the requirements.

Regarding the carbon dioxide activated wood samples, a slight increase in the SSA with increasing carbonization temperatures from 850 °C to 900 °C but a huge increase towards 1080 m^2 g^{-1} at 950 °C is noticed. Compared to steam activated samples, nitrogen physisorption isotherms (Fig. 5) with very small hysteresis loops are determined, showing smaller mesopore amounts. At this point, it has to be mentioned that the progressive carbonization at 950 °C causes a burn off of over
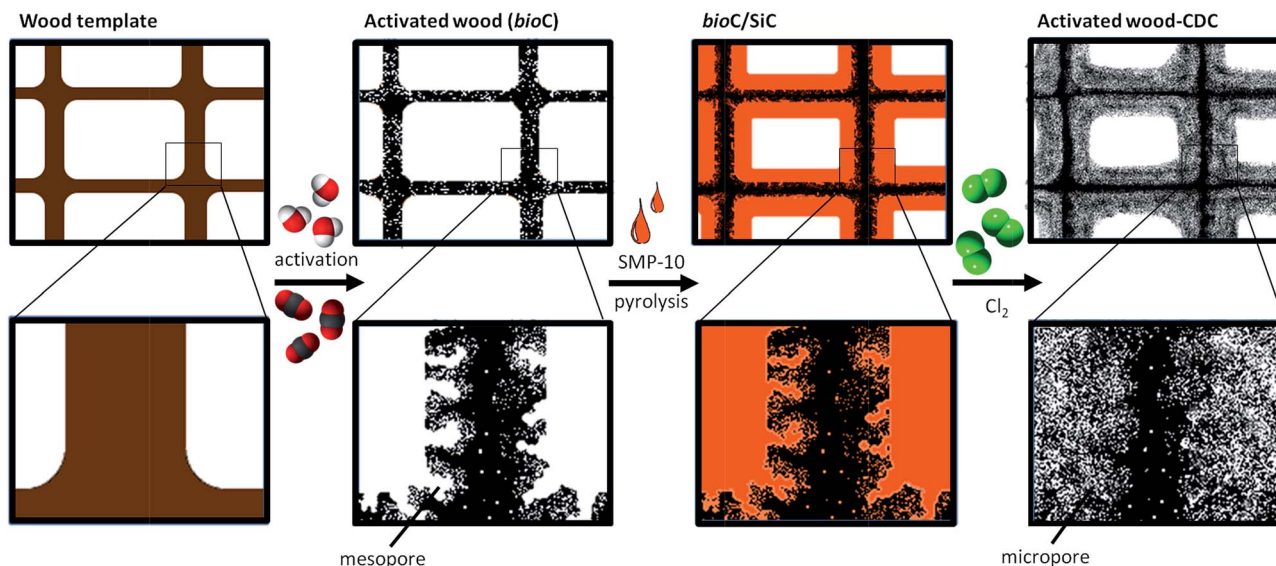
This journal is © The Royal Society of Chemistry 2015

J. Mater. Chem. A, 2015, **3**, 24103–24111 | **24105**

Fig. 1 Wood template is first activated with CO_2 or steam, resulting in activated wood (bioC) with a typical wood microstructure and additional porosity, consisting of micro- and meso-pores. Followed by impregnation of macro-, meso-, and micro-pores with polycarbosilane (SMP-10) and pyrolysis, the bioC/SiC composite is synthesized, which is treated with hot chlorine in the final synthesis step. The resulting activated wood-CDC material consists of macro-, meso-, and micro-porosity.

50%, which results in a notable broadening of pore size distribution in addition to a decreasing micropore amount and severely destroyed cell walls, presented in Fig. 3.

Activated wood-carbide-derived carbons

To receive a higher SSA, pore volumes (PV) and a small pore size distribution, the activation process was combined with the carbide-derived carbon approach.[22] Using an impregnation with pure polycarbosilane solution, the accessible macropores as well as meso- and micro-pores are filled with the silicon carbide precursor, as displayed in SEM images of the resulting CDC materials (Fig. 2f and 3d and e), as well as nitrogen physisorption isotherms and pore size distributions of the bioC/SiC composites in comparison to the non-infiltrated activated wood samples (Fig. 4a and b and 5a and c). The subsequent selective extraction of silicon atoms by chlorine treatment is associated with the formation of large amounts of micropores in the walls

Table 1 Specific surface area, pore size, and pore volume of the activated bioCs and activated wood-CDCs obtained with carbon dioxide- and steam-activation at different carbonization temperatures or with different steam saturation concentrations at 900 °C

Steam			Activated wood					Activated wood-CDC				
Water temperature, °C	Steam saturation, g m^{-3}	Burn off[a], %	SSA, m^2 g^{-1}	Micropore volume[b], cm^3 g^{-1}	Mesopore volume[b], cm^3 g^{-1}	Mesopore size, nm	Macropore size[c,d], μm	SSA, m^2 g^{-1}	Micropore volume[b], cm^3 g^{-1}	Mesopore volume[b], cm^3 g^{-1}	Mesopore size, nm	Macropore size[c,d], μm
25	23.0	3.3	670	0.28	0.06	4.9	4.0	1090	0.43	0.12	3.2	2.2
50	82.8	4.8	815	0.26	0.12	4.9	4.0	1130	0.41	0.16	3.1	2.0
80	290.7	6.1	750	0.23	0.15	5.0	4.0	890	0.30	0.23	4.4	2.0

CO$_2$		Activated wood					Activated wood-CDC				
Carbonization temperature, °C	Burn off[a], %	SSA, m^2 g^{-1}	Micropore volume[b], cm^3 g^{-1}	Mesopore volume[b], cm^3 g^{-1}	Mesopore size, nm	Macropore size[c], μm	SSA, m^2 g^{-1}	Micropore volume[b], cm^3 g^{-1}	Mesopore volume[b], cm^3 g^{-1}	Mesopore size, nm	Macropore size[c], μm
850	33.6	450	0.20	0.06	4.0	4.0	1330	0.40	0.33	3.3	2.2
900	38.6	580	0.21	0.09	4.4	4.0	1470	0.42	0.36	3.8	2.1
950	51.7	1080	0.41	0.27	6	4.5	1750	0.51	0.50	3.9	1.8

[a] Burn off: weight loss due to the activation process (weight loss due to carbonization of the wood template of about 77% is not included). [b] Pore volumes calculated from nitrogen physisorption isotherms with the QSDFT model. [c] Macropore size was determined by SEM images. [d] Macropore volumes were determined representatively with mercury porosimetry for H_2O50 and H_2O50-CDC with 1.3 and 1.2 cm^3 g^{-1}, respectively.
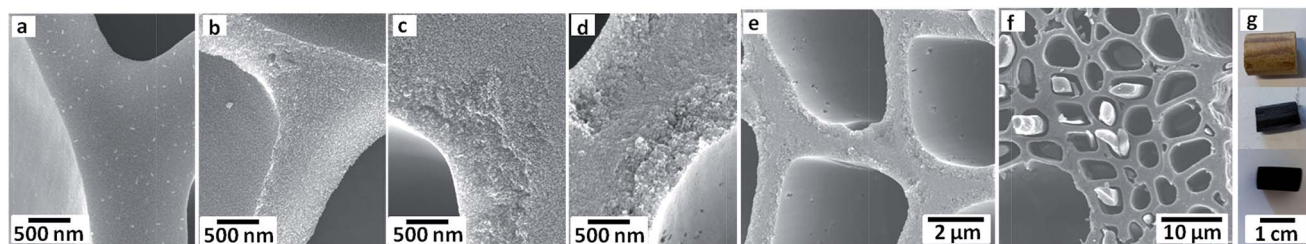
Fig. 2 SEM images of cell walls of pyrolyzed wood (a) and steam activated wood samples, activated with water of 25 °C (b), 50 °C (c), and 80 °C (d). The SEM image of steam activated wood (H_2O50) prepared with 50 °C warm water (e), and activated wood-CDC (H_2O50-CDC) (f), respectively. (g) Images of wood (top), activated wood (middle) and activated wood-CDC (bottom) monoliths.
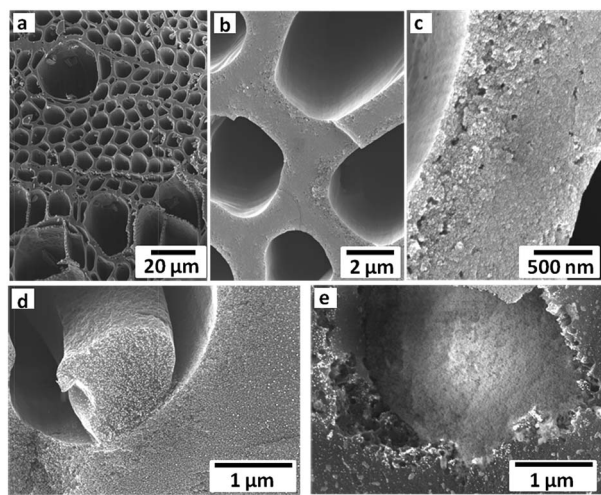

Fig. 3 (a–c) SEM images of the carbon dioxide activated wood sample, prepared at 850 °C. SEM images of the activated wood-CDC samples prepared with carbonization temperatures of 850 °C (d) and 950 °C (e), respectively.

of the amorphous silicon carbide[37] (XRD patterns of the amorphous bioC/SiC composite are shown in Fig. S1†). The carbon content of the resulting activated wood-CDC materials estimated by EDX measurements is about 95 at% (Table S1†), with only residues of silicon and oxygen. TGA measurements show complete conversion under air, which confirm the high purity of the materials (Fig. S2†). As shown in Fig. 2 and 3, macropores are still present, but partially filled with the CDC material resulting in smaller average diameters of about 2 μm. Due to insertion of the microporous CDC material in the activated wood structure, the SSA and PV are improved up to 1130 m^2 g^{-1} and 0.57 cm^3 g^{-1} (Table 1) for steam treated samples. Moreover, the trend of an optimum SSA at 50 °C water temperature and the decreasing micropore amount with increasing activation temperature is maintained. Nitrogen physisorption isotherms and pore size distributions in Fig. 4 show drastically higher amounts of micropores, determined by the distinct uptake of nitrogen in low relative pressures ($p/p_0 < 0.1$), and less small mesopores of 4–8 nm in the CDC materials compared to the activated wood materials. This decrease of 4–8 nm mesopores and the simultaneous increase of smaller mesopores could be
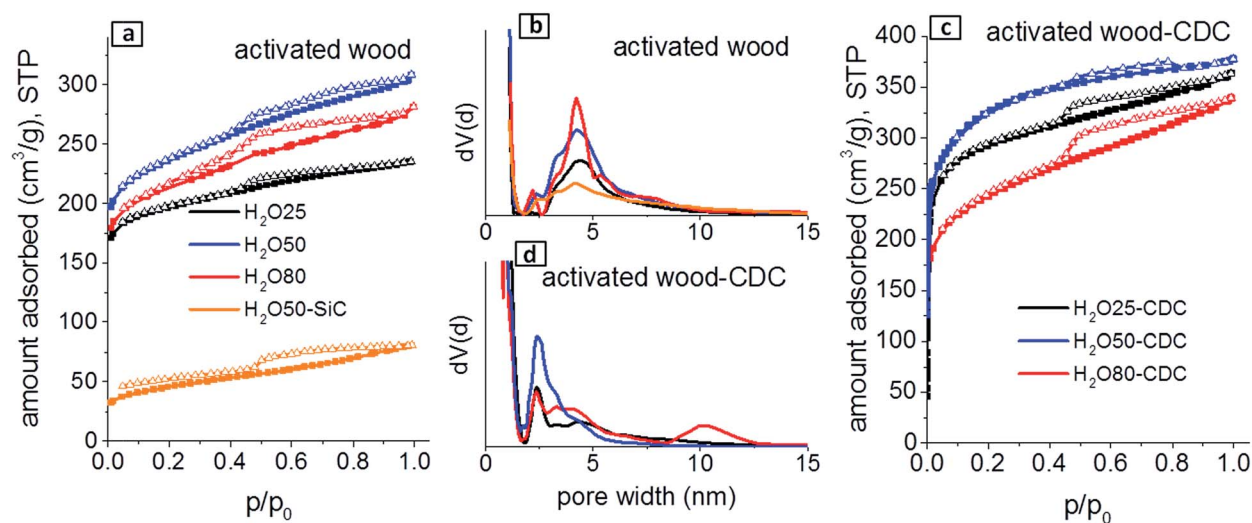

Fig. 4 (a) N_2 physisorption isotherms and (b) pore size distributions of steam activated wood samples, prepared with different steam concentrations and activated bioC/SiC prepared with steam from 50 °C warm water. (c) N_2 physisorption isotherms of activated wood-CDCs prepared with different steam concentrations and their corresponding pore size distributions (d) (STP: standard temperature and pressure).
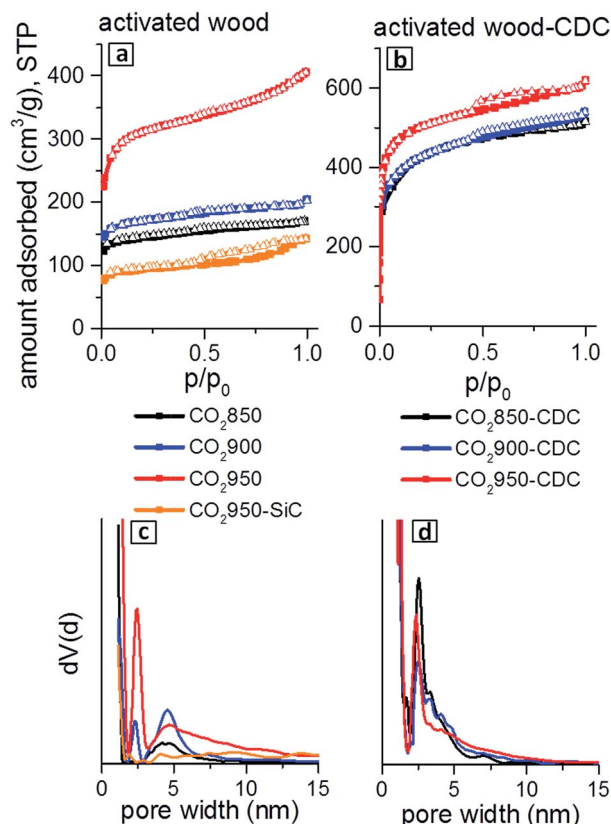
Fig. 5 (a) N_2 physisorption isotherms and (c) pore size distributions of CO_2 activated wood samples, prepared at different carbonization temperatures and activated bioC/SiC prepared with CO_2 at 950 °C. (b) N_2 physisorption isotherms of activated wood-CDCs synthesized at different carbonization temperatures and their corresponding pore size distributions (d).

explained by filling of the activated wood sample with polycarbosilane.

In the impregnation step the polycarbosilane solution penetrates into the template and fills micro-, meso-, and macro-pores. This infiltrated material ensures a narrowing or complete filling of these pores. The filling of the meso- and micro-pores with silicon carbide can be observed very well in the isotherms and associated pore size distributions, shown in Fig. 4 and 5. Regarding the data of bioC/SiC and activated bioC samples (H_2O-50 and H_2O50-SiC), the bioC/SiC composites show a significant decrease of nanopores, especially of mesopores. This leads to the narrowing of the distribution. Additional micropores are introduced in the materials by conversion of SiC into CDC by chlorine treatment, yielding higher micropore volumes for resulting CDC materials. Hence, the incorporation of the CDC material not only increases the SSA but also induces a pronounced narrowing of the pore size distribution, consisting of mainly micro- and small meso-pores. Remarkable in the pore size distributions is also a nearly similar distribution of small mesopores in all steam activated wood-CDC materials.

Regarding the carbon dioxide activated wood-CDCs, SEM images (Fig. 3) show that also CO_2 activated bioC monoliths can be combined with the CDC approach yielding in hierarchical

carbon materials. With nitrogen physisorption measurements increasing SSA and PV at higher activation temperatures with more than 1700 m^2 g^{-1} and 1 cm^3 g^{-1} were determined. CO_2 as well as steam activated wood-CDCs are characterized by micropores, small mesopores up to 10 nm, and macropores (2 μm) of the wood template. Moreover, a narrowing of the pore size distributions for activated wood-CDCs in comparison to the activated bioCs is noticed (Fig. 5). This trend could be also observed by steam activated CDC samples. To the best of our knowledge, no carbon structure obtained from a biotemplate with a trimodal pore system and very high specific surface area was described in the literature so far.

By comparing activated wood-CDCs with CDCs from non-activated wood templates (also using 100% SMP-10, showing a surface area of 940 m^2 g^{-1}),[25] it becomes evident that the activation methods prior to the CDC approach leads to an appreciable enhancement of the specific surface area without a broadening of the pore size distribution. This can be decisively attributed to the better diffusion/transport of the polycarbosilane into the wood structure *via* the inserted pores within the cell walls. The received results show that insertion of pores in the wood cell walls by the activation process is a facile and efficient method for generating a high porosity and to increase the impregnability of the wood template. Higher silicon carbide and consequently, higher CDC contents can be achieved by this increased impregnability due to the activation process, yielding high specific surface areas and pore volumes.

In conclusion, this combination of the activation process and CDC approach by impregnation of biotemplates enables the possibility to obtain highly porous carbon materials with a hierarchical trimodal pore system, high surface areas, and narrow pore size distribution for nanopores, interesting for versatile applications like catalysis, adsorption or electrochemical devices.

Electrochemical performance

The highly distinctive interconnected trimodal pore system consisting of micro-, meso-, and macro-pores should be well suitable to build up a lithium sulfur battery with excellent rate capability. Thus, steam activated wood-CDC (H_2O50-CDC) with the micro-/meso-pore volume of 0.57 cm^3 g^{-1} was evaluated in Li–S battery tests as a proof-of-principle. To investigate the influence of the prior activation process to the overall performance, a non-activated wood-CDC[25] was used as the reference material. According to the low micro-/meso-pore volume, only 28% of sulfur can be infiltrated inside the micro-/meso-pores of the reference material to maintain a sufficient void space for volume expansions during the discharge process. The increased pore volume of the steam activated material (H_2O50-CDC) enables a sulfur content of 34% without decreasing the accessibility of the well suitable pore system. The authors want to point out that for future Li–S technologies sulfur loadings of >70% are required. Here, the authors focus in a first proof-of-principle on the promising properties in rate stability of activated wood-CDCs, knowing the need for further optimization of the system, with respect to sulfur loading. However, the low

24108 | *J. Mater. Chem. A*, 2015, **3**, 24103–24111

This journal is © The Royal Society of Chemistry 2015

sulfur content of the pristine composites could be compensated by enlarging the sulfur loadings due to compression of the prepared dense electrodes. All materials infiltrated with sulfur are further labelled with _S at the end. For H_2O50-CDC_S as well as the reference, no sulfur peaks are detected in the X-ray powder diffraction pattern after melt infiltration indicating that sulfur does exist in a completely amorphous state inside the pores of both carbon materials (Fig. S4†). Nitrogen physisorption measurements before and after sulfur infiltration (Fig. S5†) also evidence the favorable distribution of sulfur inside the smaller pores rather than the larger macropores due to the decrease of the micro-/meso-pore volume. TG measurements of the melt-infiltrated samples are in good agreement with the adjusted carbon to sulfur ratio (Fig. S6†). SEM images of the compressed electrodes show a very dense and smooth surface (Fig. S7a and c†) leading to a high sulfur loading of 3 mg_{sulfur} cm^{-2} for H_2O50-CDC_S and 2 mg_{sulfur} cm^{-2} for the reference material, respectively, eliminating the disadvantage of the low sulfur content.[38,39] To optimize the overall cell performance, electrodes with high sulfur loadings as well as more importantly low electrode dead volumes are absolutely necessary (dense electrodes) to achieve practical conditions. Despite densification of the electrodes, the macroporous network was maintained (Fig. S7b and d†). In fact, these structural motifs, especially the pore geometry of wood can improve the high limitations of sulfur utilization at very high current densities due to the beneficial periodically ordered transport pores even using low excess of electrolyte. Considering that the trimodal pore system possesses unique synergetic properties, on the one hand, the micropores and small mesopores act as reaction chambers.[40] On the other hand, the macropores might improve the transport of the electrolyte, which is the most important kinetics limiting step at higher current densities. Consistently, the discharge capacities at varying current rates (Fig. 6a) show only a slight loss of capacity even at rates as high as 2C at a current density of 10.09 mA cm^{-2}. An initial discharge capacity of 865 mA h g_{sulfur}^{-1} (0.1C, 0.5 mA cm^{-2}) and a stable

capacity of over 580 mA h g_{sulfur}^{-1} (0.1C to 1C (5.05 mA cm^{-2})) were achieved for H_2O50-CDC_S, whereas the reference composite shows lower capacities. However, the trend of the chart looks similar, which is in good agreement with our findings that the main difference of both wood-derived materials is only the microporosity. Therefore, the large 3D transport pores, evolutionarily developed for optimized liquid transport over several 100 Mio years, are beneficial for low capacity losses at high C-rates and, furthermore, the micro- and meso-porosity (small mesopores) mainly influence the sulfur utilizations, leading to a synergetic trimodal pore system[41,42] with good cycle stability (Fig. 7). However, at a remarkable high current density of 25.23 mA cm^{-2} (5C) the discharge capacity starts to drop faster to 400 mA h g_{sulfur}^{-1} for H_2O50-CDC_S. The corresponding voltage profiles show low polarizations at moderate rates as can be seen from Fig. 6b (for voltage profile of reference see Fig. S8†). The rate capability, with respect to the applicable current density of H_2O50-CDC_S, especially the low loss of capacity, is an outstanding result in comparison to previous publications[32,36,43–47] with high rates.

Moreover, we only used an amount of electrolyte as low as 6.8 μL mg_{sulfur}^{-1}. The latter is essential in evaluating rate
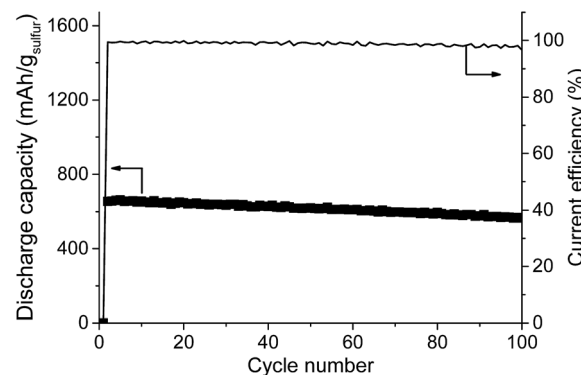

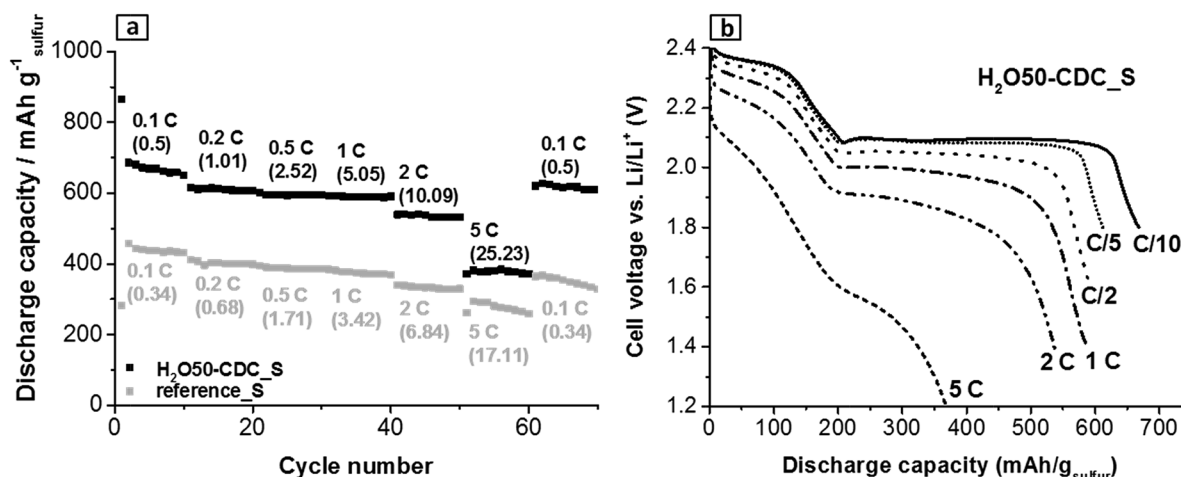
Fig. 7 Cycling stability of H_2O50-CDC.

Fig. 6 (a) Rate capability test (C/10–5C). The values in brackets represent the corresponding current densities in mA cm^{-2}; (b) typical discharge voltage profiles of the H_2O50-CDC_S composite at different rates (taken from each 5th cycle).

performance. A very high excess of electrolyte can feign a good rate performance by buffering the lithium polysulfides.[47,48] Furthermore, a high excess of lithium in combination with a high excess of electrolyte can feign good cycle performance. To our knowledge, to date no publication can achieve such a high sulfur utilization as well as discharge capacity stability at current densities exceeding 20 mA cm^{-2} even using such a low amount of electrolyte. Although other sulfur host materials applied as high rate composites showed higher sulfur utilizations, the sulfur content was very low (0.4–0.8 mg$_{sulfur}$ cm^{-2}) and faster capacity fading at increased C-rates was observed.[32,43–46] Furthermore, a huge excess of electrolyte was used leading to a low system energy density as compared to the rather realistic conditions in our approach. In contrast, the second concept from the literature with high sulfur loadings (>6 mg$_{sulfur}$ cm^{-2}) and consequently high areal capacities shows only low C-rates to avoid high current densities as well as low discharge capacities.[46] Nevertheless, even an ordered hierarchical porous carbon[36] DUT-86-2_S with micro- and meso-pores, but without macropores with similar sulfur loading shows strong capacity fading at high C-rates (over 1C), whereas the wood transport pores in wood-CDC materials can buffer further losses (Fig. S9†). Apart from that, further improvements of the wood activation process (improvement of microporosity) might increase the sulfur utilization to those levels that are achieved by benchmark materials (e.g. DUT-86-2_S) only at low rates.

Conclusions

We presented the synthesis of a trimodal hierarchical carbon by combining the activation with steam or carbon dioxide of wood templates with a subsequent CDC approach. Therefore, we mimic porous structures with cell anatomies that are optimized for mass transport during their long-term evolutional process as templates to setup the macropore structure of the material. We demonstrated that pre-treatment with steam or carbon dioxide inserts micro- and meso-pores into the wood template and that subsequent impregnation with a silicon carbide precursor and halogen treatment yields a significantly higher SSA for the activated wood-CDC material in contrast to non-activated wood-CDC. This combination of different synthesis strategies with wood templates yields activated wood-CDC materials with specific surface areas up to 1130 m^2 g^{-1} by steam activation and 1750 m^2 g^{-1} by CO$_2$ activation. They offer narrow pore size distributions in the micro- and small meso-pore range due to the activation and CDC approach, while maintaining the evolution-derived macropores of the wood template. This hierarchical biomorphic pore system ensures both efficient mass transfer and high capacities, which makes activated wood-CDCs interesting as cathode materials for Li–S batteries. The steam activated wood-CDC and a non-activated wood-CDC reveal excellent discharge capacity stability. Due to the higher surface area, pore volume and sulfur loading, higher capacities could be achieved with the activated sample. With this sample, a highly stable capacity of over 580 mA h g$_{sulfur}$$^{-1}$ at current densities exceeding 20 mA cm^{-2} (2C) with high sulfur utilization and at a very low amount of electrolyte of 6.8 μL mg^{-1} are possible.

Making use of evolutionarily developed pore systems and their functionalization could be also a promising strategy for other liquid phase applications where the subtle interplay of transport and storage requires complex hierarchical pore structures.

References

1 L. Borchardt, F. Hasche, M. Lohe, M. Oschatz, F. Schmidt, E. Kockrick, C. Ziegler, T. Lescouet, A. Bachmatiuk, B. Buechner, D. Farrusseng, P. Strasser and S. Kaskel, Carbon, 2012, 50, 1861–1870.

2 G.-P. Hao, M. Oschatz, W. Nickel, M. Adam and S. Kaskel, Curr. Org. Chem., 2014, 18, 1262–1279.

3 Y. Gogotsi, R. Dash, G. Yushin, T. Yildirim, G. Laudisio and J. Fischer, J. Am. Chem. Soc., 2005, 127, 16006–16007.

4 G. Yushin, E. Hoffmann, M. Barsoum, Y. Gogotsi, C. Howell and S. Sandeman, Biomaterials, 2006, 27(34), 5755–5762.

5 J. Chmiola, G. Yushin, Y. Gogotsi, C. Portet, P. Simon and P. Tabema, Science, 2006, 313, 1760–1763.

6 L. Borchardt, M. Oschatz and S. Kaskel, Mater. Horiz., 2014, 1, 157–168.

7 L. Borchardt, M. Oschatz, M. Lohe, V. Presser, Y. Gogotsi and S. Kaskel, Carbon, 2012, 50, 3987–3994.

8 V. Presser, M. Heon and Y. Gogotsi, Adv. Funct. Mater., 2011, 21, 810–833.

9 M. Oschatz, E. Kockrick, M. Rose, L. Borchardt, N. Kein, I. Senkovska, T. Freudenberg, Y. Korenblit, G. Yushin and S. Kaskel, Carbon, 2012, 48(14), 3987–3992.

10 H. Sieber, C. Rambo, J. Cao, E. Vogli and P. Greil, Key Eng. Mater., 2002, 206–213, 2009–2012.

11 P. Greil, T. Lifka and A. Kaindl, J. Eur. Ceram. Soc., 1998, 18, 1961–1973.

12 P. Greil, T. Lifka and A. Kaindl, J. Eur. Ceram. Soc., 1998, 18, 1975–1983.

13 T. Ota, M. Takahashi, T. Hibi, M. Ozawa, S. Suzuki and Y. Hikidi, J. Am. Ceram. Soc., 1995, 78(12), 3409–3411.

14 H. Cheng, H. Endo, T. Okabe, K. Saito and G. Zheng, J. Porous Mater., 1999, 6, 233–237.

15 M. Patel and B. Padhi, J. Mater. Sci. Lett., 1993, 12, 1234–1235.

16 W. Qiao, Y. Korai, I. Mochida, Y. Hori and T. Maeda, Carbon, 2002, 40, 351–358.

17 Z. Jin and G. Zhao, BioResources, 2014, 9(2), 2237–2247.

18 Z. Jin and G. Zhao, BioResources, 2014, 9(4), 6831–6840.

19 A. R. Sanchez, A. A. Elguezabal and L. de La Torre Saenz, Carbon, 2001, 39, 1367–1377.

24110 | J. Mater. Chem. A, 2015, 3, 24103–24111

This journal is © The Royal Society of Chemistry 2015

20 F.-C. Wu, R.-L. Tseng and R.-S. Juang, *Sep. Purif. Technol.*, 2005, **47**, 10–19.

21 N. Tancredi, T. Cordeo, J. Rodriguez-Mirasol and J. J. Rodriguez, *Sep. Sci. Technol.*, 1997, **32**(6), 1115–1126.

22 Y. Gogotsi, A. Nikitin, H. Ye, W. Zhou, J. Fischer, B. Yi, H. Foley and M. W. Barsoum, *Nat. Mater.*, 2003, **2**, 591–594.

23 L. Borchardt, C. Hoffmann, M. Oschatz, L. Mammitzsch, U. Petasch, M. Herrmann and S. Kaskel, *Chem. Soc. Rev.*, 2012, **41**, 5053–5067.

24 M. Oschatz, L. Borchardt, M. Thommes, K. A. Cychosz, I. Senkovska, N. Klein, R. Frind, M. Leistner, V. Presser, Y. Gogotsi and S. Kaskel, *Angew. Chem., Int. Ed.*, 2012, **51**(13), 7577–7580.

25 M. Adam, M. Oschatz, W. Nickel and S. Kaskel, *Microporous Mesoporous Mater.*, 2015, **210**, 26–31.

26 B. Scrosati, J. Hassoun and Y. K. Sun, *Energy Environ. Sci.*, 2011, **4**, 3287–3295.

27 P. G. Bruce, S. A. Freunberger, L. J. Hardwick and J.-M. Tarascon, *Nat. Mater.*, 2012, **11**, 19–29.

28 A. Manthiram, S. H. Chung and C. Zu, *Adv. Mater.*, 2015, **27**, 1980–2006.

29 X. Ji, K. T. Lee and L. F. Nazar, *Nat. Mater.*, 2009, **8**, 500–506.

30 X. Ji and L. F. Nazar, *J. Mater. Chem.*, 2010, **20**, 9821–9826.

31 H. Yao, G. Zheng, P. C. Hsu, D. Kong, J. J. Cha, W. Li, Z. W. She, M. T. McDowell, K. Yan, Z. Liang, V. K. Narasimhan and Y. Cui, *Nat. Commun.*, 2013, **5**, 3943.

32 Z. Wei Seh, W. Li, J. J. Cha, G. Zheng, Y. Yang, M. T. McDowell, P.-C. Hsu and Y. Cui, *Nat. Commun.*, 2013, **4**, 1331.

33 M. Rose, Y. Korenblit, E. Kockrick, L. Borchardt, M. Oschatz, S. Kaskel and G. Yushin, *Small*, 2011, **7**(8), 1108–1117.

34 M. Oschatz, S. Thieme, L. Borchardt, M. R. Lohe, T. Biemelt, J. Brückner, H. Althues and S. Kaskel, *Chem. Commun.*, 2013, **49**, 5832–5834.

35 S. Thieme, J. Brückner, I. Bauer, M. Oschatz, L. Borchardt, H. Althues and S. Kaskel, *J. Mater. Chem. A*, 2013, **1**, 9225.

36 C. Hoffmann, S. Thieme, J. Brückner, M. Oschatz, T. Biemelt, G. Mondin, H. Althues and S. Kaskel, *ACS Nano*, 2014, **8**(12), 12130–12140.

37 M. Oschatz, L. Borchardt, K. Pinkert, S. Thieme, M. R. Lohe, C. Hoffmann, M. Benusch, F. M. Wisser, C. Ziegler, L. Giebeler, M. H. Rümmeli, J. Eckert, A. Eychmüller and S. Kaskel, *Adv. Energy Mater.*, 2014, **4**, 1300645–1300648.

38 L. X. Miao, W. K. Wang, A. B. Wang, K. G. Yuan and Y. S. Yang, *J. Mater. Chem. A*, 2013, **1**, 11659–11664.

39 M. Wang, W. Wang, A. Wang, K. Yuan, L. Miao, X. Zhang, Y. Huang, Z. Yu and J. Qiu, *Chem. Commun.*, 2013, **49**, 10263–10265.

40 P. Strubel, S. Thieme, T. Biemelt, A. Helmer, M. Oschatz, J. Brückner, H. Althues and S. Kaskel, *Adv. Funct. Mater.*, 2015, **25**, 287–297.

41 X. Li, Y. Cao, W. Qi, L. V. Saraf, J. Xiao, Z. Nie, J. Mietek, J.-G. Zhang, B. Schwenzer and J. Liu, *J. Mater. Chem.*, 2011, **21**, 16603.

42 C. Liang, N. J. Dudney and J. Y. Howe, *Chem. Mater.*, 2009, **21**, 4724–4730.

43 X. Yang, L. Zhang, F. Zhang, Y. Huang and Y. Chen, *ACS Nano*, 2014, **8**(5), 5208–5215.

44 G. He, X. Ji and L. Nazar, *Energy Environ. Sci.*, 2011, **4**, 2878–2883.

45 J. Schuster, G. He, B. Mandlmeier, T. Yim, K. T. Lee, T. Bein and L. F. Nazar, *Angew. Chem., Int. Ed.*, 2012, **51**, 3591–3595.

46 L. Miao, W. Wang, K. Yuan, Y. Yang and A. Wang, *Chem. Commun.*, 2014, **50**, 13231–13234.

47 J. Brückner, S. Thieme, H. T. Grossmann, S. Dörfler, H. Althues and S. Kaskel, *J. Power Sources*, 2014, **268**, 82–87.

48 L. F. Nazar, M. Cuisinier and Q. Pang, *MRS Bull.*, 2014, **39**, 436–442.